Lunar Soil Sample 15421,67 – Stranger Things. D. C. Barker[1], J. E. Snow[1] and G. Costin[2], [1]Department of Earth and Atmospheric Sciences, University of Houston, Science & Research Building 1, 3507 Cullen Blvd, Rm. 312. Houston, Texas 77204), [2]Department of Earth, Environmental and Planetary Sciences, Rice University, 6100 Main Street, Houston, TX, 77005.

Introduction: As part of an ongoing effort examining the ubiquitous Apollo 15 (Spur Crater, Station 7) glasses we also handpicked many grains with a uniquely different morphology and briefly examined them in parallel. Four of these grains from lunar sample 15421,67 were analyzed using a combination of EPMA (quantative major elements) and qualitative EDS and BSE. The UH JEOL JSM-6330F SEM and LSX213-Varian 810 LAICPMS, and Rice JEOL JXA 8530F microprobe were used for these analysis. Table 1 provides EPMA analysis for the individual grain analysis.

1) 15421,67 Metal Fragment: Figure 1 shows a 1200 µm metal fragment (#S13B1), exhibiting fracture morphology suggestive of sheared metal. Traditional sources of metal particles in lunar soil come from meteoritic matter and native sources [1,2]. The formula for this grain is: $(Fe_{1.287}Ni_{0.143}Mn_{0.023}Cu_{0.006})_{\sum=1.459}Cr_{0.351}$, which is close to chromferide (ideal formula - $Fe_{1.5}Cr_{0.2}$ IMA1984-021). However, it could also be a sliver from the EVA Tongs or Adjustable Scoop [3] being composed of 17-4 and 17-7 Ph stainless steels respectively [4]. Yet, the average composition and 2-sigma error for Cr, Ni, Mn and Cu reside outside published production steel standards. Further, the second image shows exsolution of MnS rich dark regions, uncommon in stainless steel. This piece of metal remains a stranger thing.

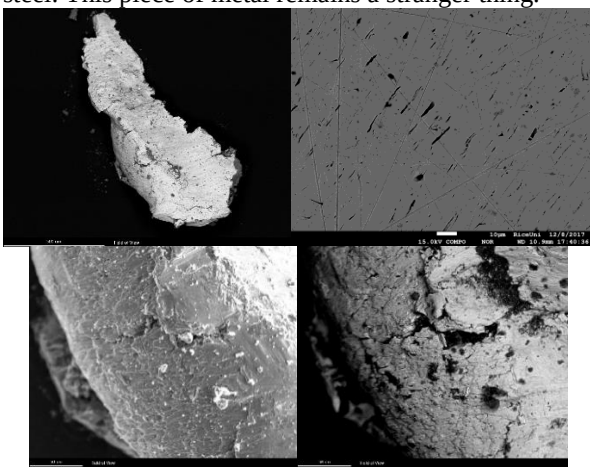

Fig. 1 SE (left) and BSE (rt) images of metal fragment.

2) 15421,67 Impact Melt Grain: This transparent greenish, 500 µm long fragment (#S7B9) is the only grain of over 85 chosen that seems to be a glass other than of volcanic origin [5,6,7]. This quenched basalt glass (Mg# of 70.26) contains rounded inclusions of 96% silica glass (Fig. 2), which themselves contain fragments (~5 µm) of rutile and almandine. This silica glass may possibly be a high pressure impact melt remnant, e.g., shocked silica/anothite [8]. Both the SiO_2 glass and the larger isolated almandine crystals seem to have been later incorporated within a basaltic melt that was also crystallizing zoisite phenocrysts $(Ca_{1.940}Mg_{0.017}Na_{0.002}Mn_{0.002})_{\sum=2.000}$ $(Al_{2.554}Fe^{3+}_{0.376}Fe^{2+}_{0.074}Ti_{0.008})_{\sum=3.010}$ $[Si_{1.00}O_4][Si_{2.03}O_7]O(OH)$, before the complete assemblage was quenched.

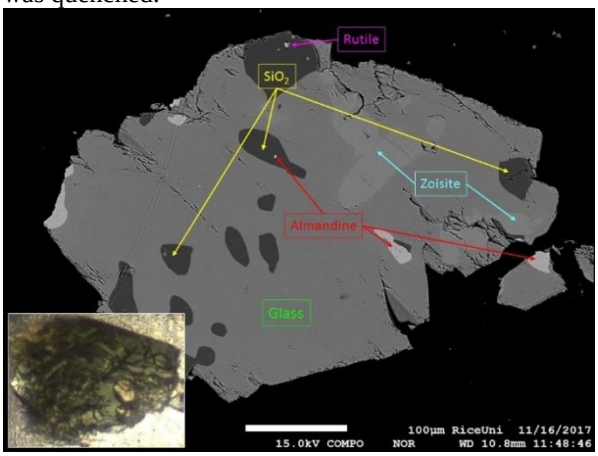

Fig. 2 Optical and BSE image of basalt glass.

3) 15421,67 Lunar Anorthosite Fragment: Figure 3 shows a 1070 µm wide transparent fragment (#S9B1) containing pyroxene/augite ($En_{42}Wo_{36}Fs_{22}$) fragments exhibiting complete lamellar exsolution, phenocrysts of euhedral olivine ($Fo_{55}Fa_{45}$), ilmenite and hypersthene ($En_{62}Fs_{34}Wo_3$). All modal proportions are roughly equal within a matrix of anorthite ($An_{95}Ab_5$). Figure 4 shows the CI normalized trace element data for three parts of this assemblage (gaps indicate no detection). It is interesting to note the positive Eu spike in both olivine and anorthite and the negative Eu anomoly in the hypersthene (labeled Opx).

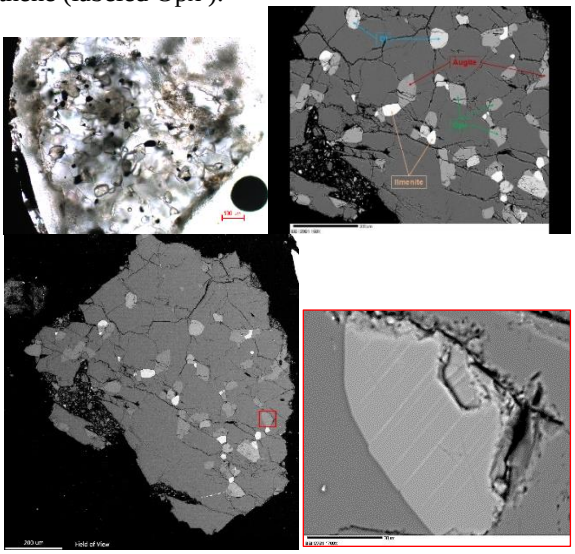

Fig. 3 Optical/BSE images of anorthosite fragment.

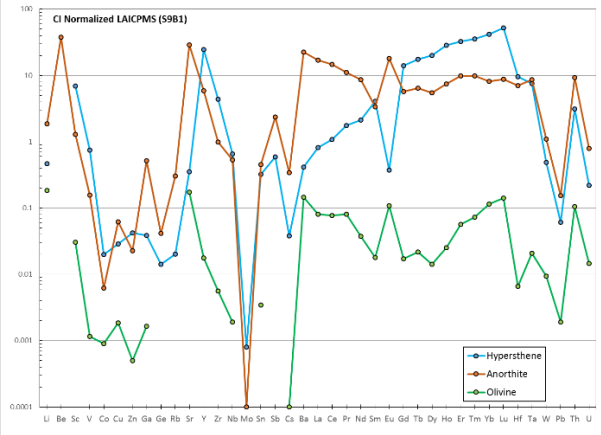

Fig. 4 #S9B1 LAICPMS analysis; error < 5%.

4) 15421,67 Monocrystal Fragment: A single 462 µm long pyroxene fragment (#S11B9) was found to contain microscopic exsolution lamellae after (100) and (001) planes [9], whose composition varies between a hypersthene host ($En_{60}Fs_{37}Wo_3$) and darker augite ($Wo_{44}En_{41}Fs_{15}$) lamellae and larger masses, bracketed by chromite and possibly olivine and ilmenite (unreported bright spots). The small lamellae size range (< 5 µm) indicates rapid cooling, and may be interpreted as having formed at a shallow burial depth (< 0.5 km) in the anorthosite crust of the Moon [10]. Figure 6 shows the CI normalized trace element data (50 µm beam size) with a large negative Eu as expected from the crust.

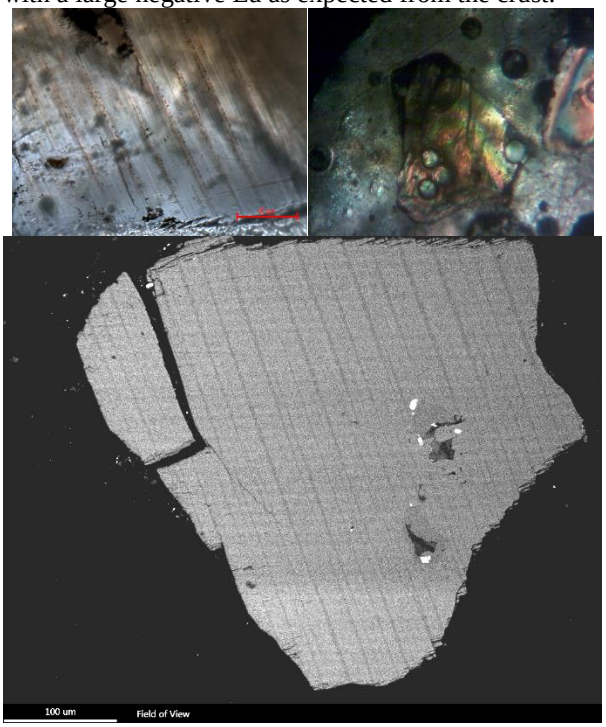

Fig. 5 Optical and BSE images of pyroxene monocrystal fragment showing exsolution lamallae – dark lamelle are augite in a lighter hypersthene host.

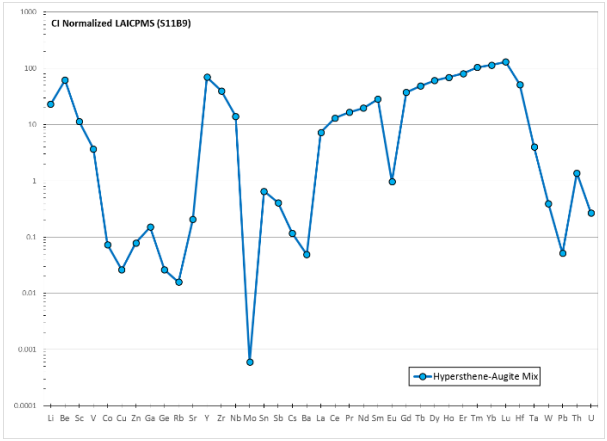

Fig. 6 #S11B9 LAICPMS analysis ; error < 5%.

EPMA Data:

Fe	Cr	Ni	Mn	Cu	Si	Ti	Zn	S	Ta	--	--	--	Total	Minerals
S13B1														
71.88	18.24	8.37	1.25	0.41	0.29	0.01	0.02	0.02	0.00	--	--	--	100.48	Chromferride
SiO_2	**TiO_2**	**Al_2O_3**	**Cr_2O_3**	**FeO**	**MnO**	**MgO**	**CaO**	**Na_2O**	**K_2O**	**NiO**	**P_2O_5**	**SO_3**	**Total**	**Minerals**
S7B9														
48.81	0.39	10.87	0.01	10.37	0.03	13.74	9.42	3.02	0.43	--	0.01	0.00	97.10	Basaltic Glass
96.19	0.04	0.00	0.01	0.26	0.00	0.01	0.01	0.00	0.00	0.01	--	--	96.90	SiO_2 Glass
38.71	0.13	27.69	0.01	6.92	0.02	0.14	23.15	0.01	0.00	0.01	--	--	96.80	Zoisite
38.12	0.10	21.32	0.00	26.76	0.77	4.59	7.79	0.04	0.00	0.02	--	--	99.50	Almandine
				S9B1							**V_2O_3**	**ZnO**		
44.53	0.02	35.80	0.01	0.19	0.01	0.04	19.07	0.53	0.02	0.00	--	--	99.14	Anorthite
0.01	54.22	0.01	0.09	42.73	0.55	2.76	0.17	0.01	0.00	0.03	0.00	0.03	98.76	Ilmenite
35.25	0.05	0.02	0.01	37.02	0.43	25.26	0.13	0.01	0.01	0.00	--	--	99.53	Olivine
52.42	0.45	0.82	0.30	21.20	0.35	21.39	1.43	0.01	0.00	0.00	--	--	98.60	Hypersthene
52.07	0.90	1.47	0.42	12.90	0.22	13.69	16.04	0.04	0.00	0.00	--	--	99.08	Augite
							S11B9				**V_2O_3**	**ZnO**		
50.49	0.40	0.56	0.36	24.59	0.43	20.29	1.26	0.01	0.00	0.01	--	--	98.39	Hypersthene
49.28	1.19	2.62	0.83	9.95	0.24	13.66	20.27	0.18	0.00	0.01	--	--	98.22	Augite
2.85	1.27	15.08	43.64	32.11	0.39	3.87	0.17	--	--	0.00	0.21	0.02	99.60	Chromite

Table 1 Average EPMA in wt.%.

Discussion: Many small fragments within our 15421,67 aliquot uniquely stood out from the green glasses. The first, metal fragment S7B9 is believed to be naturally occurring; yet, the potential of it having been a tool fragment indicates potential for sample contamination issues, and illustrates a future need to carefully consider surface operations and to track construction materials so as to protect sample and site integrity. The rest of the grains remain interesting and yet seem representative of known lunar geological processes. Additional investigations using techniques such as Raman spectroscopy and XRD, would further constrain mineral assemblage identificaiton. Examining the unknown remains the hallmark of science and exploration, and determining future surface resource potential will require a more thorough quantification of these fine grained, easily accessible materials.

References: [1] Morris, R. V. (1980) LPSC XI, 1697–1712. [2] Wlotzka, F. et al. (1972) Proc. 3rd Lunar Sci. Conf., 1, 1077-1084. [3] Allton, J. H. (1989) JSC-23454. [4] AK Steel Material Data Sheets (www.aksteel.com). [5] Delano J. W. (1986) Proc. 16th Lunar Planet. Sci. Conf., pp. D201–D213. [6] Ryder et al. (1996) Geo. et Cosmo. Acta, 60, 4, pp. 693-710. [7] Delano and Livi (1981) Geo. et Cosmo. Acta, 45, pp. 2137-2149. [8] Miura, Y. and Graham, R. A. (1994) Shock Waves, 3, 4, pp. 293-298. [9] Grove, T. L. (1982), Amer. Min., 67, pp. 251-268. [10] Jolliff et al. (1999) Amer. Min., 84, pp. 821-837.